The movement of single large bubbles in closed vertical tubes

By H. L. GOLDSMITH AND S. G. MASON

Physical Chemistry Division, Pulp and Paper Research Institute of Canada, and Department of Chemistry, McGill University, Montreal, Canada

(Received 13 September 1961 and in revised form 23 February 1962)

The flow and deformation of single large air and liquid bubbles suspended in wetting liquids when moving under gravity in closed vertical tubes have been studied. The flow patterns in both phases and thickness of the liquid film surrounding the bubbles and the shape of the bubble ends were determined by direct observation through a microscope.

Quantitative agreement with a theory relating bubble velocity to film thickness in viscous flow, and to the tube radius in inertial flow was obtained. In viscous flow the deformation at a given interfacial tension was independent of bubble length and of the viscosity of the suspending liquid.

In viscous flow the end of the sedimenting bubbles were spheroidal, with the leading ends prolate and the trailing ends generally oblate. The axis ratio of the leading ends increased with increasing interfacial tension. Wave disturbances occurred at the trailing ends of the bubbles. In inertial flow the leading ends of rising air bubbles were hemispherical.

1. Introduction

The investigation being reported here is one of a series on the behaviour of individual particles suspended in liquids flowing through tubes. The movement of single fluid drops in liquids in laminar flow has been described by the present authors for the cases in which (*a*) the tube diameter is much larger than the undistorted drop (1962*a*), and (*b*) it is much smaller (1962*b*). This paper deals with the problem, related to the second case, of a fluid bubble which moves through a stationary liquid in a closed vertical tube under the action of gravity.

Apart from their intrinsic interest, the phenomena are of importance in connexion with heat transfer through liquids flowing down walls (Grimley 1945; Dukler & Bergelin 1952), the air bubble viscometer (Marshall 1917, p. 728), two-phase flow through porous media, such as intrusion of water into oil-bearing strata (Gardesen 1930) and of air into water-saturated networks of fibres in papermaking (Gavelin 1954), the flow of emulsions through narrow capillaries (Richardson 1953), the deformation of red blood cells during flow through the capillary system of the body and other problems.

In both flowing and sedimenting bubble systems, it has been demonstrated that when the suspending liquid wets the wall, the movement of the bubble takes place inside a film of the liquid. Measurements of the thickness of this film have

been made by electrical conductivity (Grimley 1945; Dukler & Bergelin 1952; Marchessault & Mason 1961) and directly (Gibson 1913; Davies & Taylor 1950), but these methods did not permit the investigation of liquid flow in the film and the bubble. In the present work it was possible to measure the film thickness and velocity profiles directly in systems undergoing creeping flow, and to compare the results with the simple theory developed in § 2.1. In addition, observations were made of the shape of the bubble ends, and of behaviour in bubbles at high Reynolds numbers.

2. Theoretical part

2.1. *Viscous flow*

Consider a bubble of viscosity η_1 and density ρ_1 rising ($\rho_1 < \rho_2$) or falling ($\rho_1 > \rho_2$) in a liquid (η_2, ρ_2) contained in a closed vertical tube of radius R with a velocity V_b. At positions sufficiently far removed from the ends of the bubble we can assume parallel incompressible creeping flow. Under these circumstances, the Navier–Stokes equation governing movement in the bubble and the surrounding film is, in cylindrical co-ordinates,

$$-\frac{\partial P_{1,2}}{\partial x}+\rho_{1,2}g+\frac{\eta_{1,2}}{r}\frac{\partial}{\partial r}\left(r\frac{\partial v_{1,2}}{\partial r}\right)=0, \tag{1}$$

where r is the radial distance from the tube axis, x is measured along the tube axis, and $v_1(r)$ and $v_2(r)$ are the respective velocities in the bubble and the surrounding film, the downward direction being positive. It follows from the continuity equation that the film thickness h is constant in the region where (1) holds.

Laplace's capillary equation for the pressure discontinuity at the interface is

$$P_1(x) = P_2(x)+\gamma/(R-h), \tag{2}$$

where γ is the interfacial tension of the bubble, from which it follows that

$$\partial P_1/\partial x = \partial P_2/\partial x = H, \tag{3}$$

and the general solution of (1) is

$$v_{1,2}(r) = \{(-\rho_{1,2}g+H)\,r^2/4\eta_{1,2}\}+A_{1,2}\log_e r+B_{1,2}. \tag{4}$$

The five constants of integration in (4) can be evaluated from the following boundary conditions:

(i) $v_1(0)$ is regular; hence $A_1 = 0$.

(ii) There is no slip at the wall of the tube, i.e. $v_2(R) = 0$.

(iii) The continuity requirements for flow in the bubble and film respectively are

$$\pi(R-h)^2 V_b = \int_0^{R-h} 2\pi r v_1(r)\,dr \tag{5}$$

$$= -\int_{R-h}^{R} 2\pi r v_2(r)\,dr. \tag{6}$$

(iv) The velocity is continuous at the bubble interface, i.e. $v_1(R-h) = v_2(R-h)$.

(v) The fluid shear stress is continuous at the interface, i.e. at $r = (R-h)$,

$$\eta_1\,\partial v_1/\partial r = \eta_2\,\partial v_2/\partial r. \tag{7}$$

Substituting for $v_1(r)$ from (4) into (5) and integrating yields

$$V_b = (-\rho_1 g + H)(R-h)^2/8\eta_1 + B_1, \tag{8}$$

and equation (4) for flow in the bubble is then

$$v_1(r) = (-\rho_1 g + H)\{2r^2 - (R-h)^2\}/8\eta_1 + V_b. \tag{9}$$

Applying boundary condition (ii) to (4), the equation for flow in the film is

$$v_2(r) = -\left[\frac{(-\rho_2 g + H)(R^2 - r^2)}{4\eta_2} + A_2 \log_e \frac{R}{r}\right] \tag{10}$$

and substituting $v_2(r)$ in (6) yields

$$V_b = \frac{(-\rho_2 g + H)}{\eta_2}\left[\frac{R^4}{8(R-h)^2} - \frac{R^2}{4} + \frac{(R-h)^2}{8}\right] - A_2 \log_e \frac{R}{(R-h)} + \frac{A_2[R^2 - (R-h)^2]}{2(R-h)^2}. \tag{11}$$

Applying boundary condition (v) to (9) and (10) yields on reduction

$$A_2 = -\{(\Delta\rho)\, g(R-h)^2\}/2\eta_2, \tag{12}$$

where $\Delta\rho = (\rho_1 - \rho_2)$. An expression for H is obtained by imposing boundary condition (iv) on (9) and (10)

$$H = \{(\rho_2 L + \rho_1) g + M\}/(1+L) \tag{13}$$

where

$$L = 2p\left[\frac{R^2}{(R-h)^2} - 1\right], \tag{14}$$

$$M = \left[4(\Delta\rho)\, gp \log_e \frac{R}{(R-h)} - \frac{8\eta_1 V_b}{(R-h)^2}\right] \tag{15}$$

and the viscosity ratio $p = \eta_1/\eta_2$.

Thus since A_2 and H have been evaluated, it is possible by substitution of (12) to (15) in (9) to (11) to obtain explicit expressions for $v_1(r)$, $v_2(r)$ and V_b as functions of $\rho_{1,2}$, $\eta_{1,2}$, R and h by means of which the theory can be tested. The resulting equations are cumbersome and are not set forth here. They have, however, been used for the calculations which have been compared with the experiments described later.

The velocity profiles in both phases are shown schematically in figure 1(*a*). The gradient $\partial v/\partial r$ in the bubble vanishes at $r = 0$, and in the film at $r = (R - h_0)$. Inserting the latter condition in (10) yields as a solution for h_0

$$h_0 = R - \left[\frac{(\Delta\rho) g}{-\rho_2 g + H}\right]^{\frac{1}{2}} (R-h). \tag{16}$$

There are two special cases of interest.

Case (i): inviscid bubbles. When $\eta_1 = p = 0$, (13) reduces to

$$H_0 = \rho_1 g \tag{17}$$

and $h = h_0$ (figure 1(*b*)). Upon substituting for H_0 and A_2 in (10) and (11) one obtains

$$v_2(r) = -\frac{(\Delta\rho) g}{4\eta_2}\left[(R^2 - r^2) - 2(R-h)^2 \log_e \frac{R}{r}\right] \tag{18}$$

and

$$V_b = \frac{(\Delta\rho) g}{2\eta_2}\left[\frac{R^4}{4(R-h)^2} - R^2 + \tfrac{3}{4}(R-h)^2 + (R-h)^2 \log_e \frac{R}{(R-h)}\right]. \tag{19}$$

Allowing $p \to 0$ in (9) yields $v_1(r) = V_b$. This is not a regular solution, however, since boundary condition (iv) is not satisfied, but its neglect is consistent with the assumption of zero viscosity in the bubble.

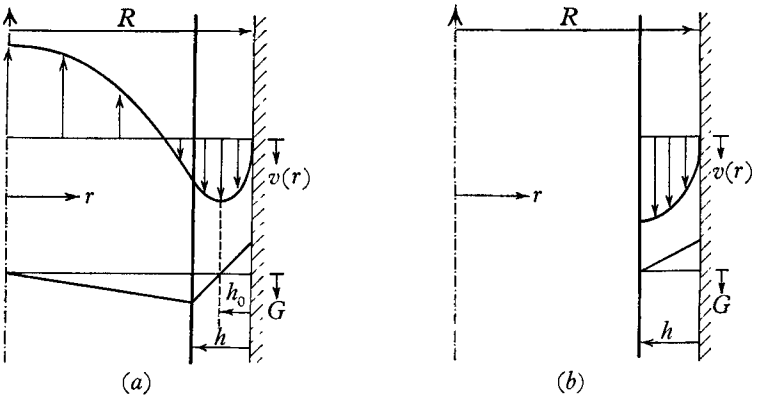

FIGURE 1. Schematic drawing of velocity profiles and gradients in rising bubble and surrounding film. (*a*) $p > 0$. The velocity gradient $G = \partial v/\partial r$ vanishes in the bubble at $r = 0$, and in the film at $r = (R-h_0)$. (*b*) $p = 0$. Here $G = 0$ at the interface, $r = (R-h)$.

Case (*ii*): $h \ll R$. Here the Navier–Stokes equation for two-dimensional planar flow in the film may be used

$$-\frac{\partial P_2}{\partial x}+\rho_2 g+\eta_2\frac{\partial^2 v_2}{\partial r^2}=0, \tag{20}$$

and by the argument used above leads to the corresponding simpler solutions

$$V_b=\frac{(-\rho_2 g+H)}{\eta_2}\frac{h^2}{R}(h_0-\tfrac{1}{3}h) \tag{21}$$

and, when $p = 0$,

$$V_b = 2(\Delta\rho)gh^3/3\eta_2 R. \tag{22}$$

Equation (22) was derived by Nusselt (1916).

It has so far not been possible to derive an analytic expression for V_b in terms of R, η_2 and the interfacial tension γ. From an experimental study of rising air bubbles in the viscous flow region Barr (1926) concluded that there was no simple relation between V_b and η_2, or between V_b and R since the surface tension was operative in determining the bubble shape. However, at a given R and γ the ratio $V_b\eta_2/(\Delta\rho)$ was approximately constant. From dimensional considerations he obtained the relation

$$V_b\eta_2/K = f(K/\gamma), \tag{23}$$

where $K = (\Delta\rho)gD^2$ and D is the tube diameter. In an analysis of his own results and those of other workers (Faust 1919; Abrams, Kavanagh & Osmond 1921; Schulz 1929), Barr showed that (23) has two limiting forms:

(1) When $(K/\gamma) > 40$, $f(K/\gamma)$ is independent of K/γ and at a given η_2, V_b is proportional to D^2.

(2) When $(K/\gamma) < 0{\cdot}6$, $V_b = 0$ and the bubble appears to stick to the tube. In the intermediate region $f(K/\gamma)$ increases very rapidly with (K/γ).

Bretherton (1961) in a quantitative treatment of bubble rise based on the lubrication approximation has given an expression relating V_b, R, η_2 and γ for small values of $\eta_2 V_b/\gamma$. Bretherton predicted that when $K/\gamma < 3{\cdot}37$ bubble flow stops or becomes unsteady, and when K/γ is slightly greater than the critical value the following equations hold

$$\frac{K/\gamma - 3{\cdot}37}{4} = 1{\cdot}10(h/R)^{\frac{2}{3}} + 1{\cdot}85(h/R)$$
$$= 1{\cdot}25(\eta_2 V_b/\gamma)^{\frac{2}{3}} + 2{\cdot}24(\eta_2 V_b/\gamma)^{\frac{1}{2}}. \tag{24}$$

2.2. *Inertial flow*

The case of an air bubble rising in an inviscid liquid ($\eta_2 = 0$) contained in a tube has been treated by Davies & Taylor (1950) and Dumitrescu (1943). At the interface the velocity of the falling liquid is given by Bernoulli's equation

$$v_2 = (2gx)^{\frac{1}{2}}. \tag{25}$$

It follows from (25) that the film thickness is no longer constant between the ends of the bubble as in viscous flow but may be expected to decrease as the inverse square root of the distance from the vertex. Davies & Taylor (1950), starting with the observation that the advancing end of a rising air bubble in an inviscid liquid has a spherical contour, have shown in a theoretical analysis that the bubble velocity is given by

$$V_b = -\beta/(gR)^{\frac{1}{2}}, \tag{26}$$

where β has the value of 0·464. Dumitrescu (1943) arrived independently at the same result, also assuming a spherical contour for the bubble head, and showed that $\beta = 0{\cdot}496$. Further, neglecting the boundary layer at the wall, Davies & Taylor (1950) showed that below $1{\cdot}5R$ from the vertex, where the horizontal component of flow becomes so small that $V_b \simeq v_2$, β may be obtained from the film thickness by the relation

$$\beta = 2\sqrt{2}(h/R)\,(x/R)^{\frac{1}{2}}. \tag{27}$$

In the experiments described below equations (9) to (11), (18) and (19) for viscous flow, and (26) and (27) for inertial flow, were tested in a number of systems.

3. Experimental part

3.1. *General*

The bubbles studied were introduced into vertical 45 cm lengths of precision-bore glass tubing containing liquids of different viscosities, and were viewed through the travelling microscope previously described (Goldsmith & Mason 1962*a*). All observations were made in the median plane of the tube normal to the viewing axis. To eliminate optical distortion by the glass wall a portion of the tube passed through a rubber stopper into a square metal-glass cell having flat viewing faces on opposite sides and containing a mixture of 60 % dibutyl phthalate and 40 % Ucon oil having the same refractive index as glass ($n_D = 1{\cdot}474$). This enabled distortion-free viewing inside the tube over a length of 30 cm. When the tube was properly aligned with the axis of travel of the microscope (within 0° 1′ of the true vertical) the bubble-liquid and glass-liquid interfaces appeared as sharp lines in

the microscope field. Using a calibrated micrometer eyepiece the film thickness was readily measured. With liquids in the tube of refractive index different from that of glass a refraction correction was applied to give the true film thickness; this correction varied from 0 to 25 % depending on the liquid and the tube radius. With a 15 × eyepiece and a 5 cm focal length objective the resolution was better than 5 μ; this was generally less than $0{\cdot}03h$.

Air bubbles of various lengths were introduced at its lower end through a side arm which was afterwards closed off from it by a pinch clamp. Liquid bubbles for which $\rho_1 > \rho_2$ were injected into the top of the tube by means of a syringe; when $\rho_1 < \rho_2$ a syringe containing the bubble liquid was directly attached to the base of the tube. The tubes were closed at the bottom, and the bubbles were viewed as they travelled past the microscope at rest. V_b was measured by observing the time of rise or fall through a known distance using a cathetometer, and l_b was calculated from the time of travel of the bubble past the cross-hairs of the cathetometer eyepiece.

For the experiments on the rise of air bubbles in inviscid liquids, the tubes were mounted vertically in a reservoir of the liquid, and were filled by suction from the top and then closed off. The reservoir was then removed and the tube allowed to empty out. The rate of rise of the upper end of the 'infinitely' long bubble thus created was measured in the usual manner.

3.2. *Bubble shapes*

The contours of the leading and rear ends of the bubbles were photographed using a 35 mm Praktika reflex camera with a 75 mm lens and extension tubes to obtain suitable magnification. They were analysed by projecting the negative onto a drafting table.

3.3. *Velocity profiles*

The velocity profiles $v_1(r)$ and $v_2(r)$ were measured by introducing aluminium tracer particles into the appropriate phase and taking cine films through the microscope (at rest) as the bubble moved past. A Paillard Bolex 16 mm cine camera was used at speeds ranging from 16 to 32 frames/second. The film was projected onto a screen and the movement of particles occurring in a given number of frames measured at various distances between the bubble and the glass wall. With silicone oil as the continuous phase, a large area of the film was obscured by internal reflexion at the glass-oil interface and the tracer particles rendered invisible. This was due to the large difference in refractive index between the oil and the glass ($-0{\cdot}07$). The difficulty was overcome by substituting the silicone oil for that normally used in the glass-metal cell. A small correction for refraction by the glass alone was made.

3.4. *Materials*

Precision-bore glass tubes (Wilmad Glass Co., Buena, N.J.) of $R = 0{\cdot}200$ to $0{\cdot}500 \pm 0{\cdot}0005$ cm were used.

The systems investigated and their relevant properties are listed in table 1. Systems 1 to 6 and 10 to 12 provided sedimenting bubbles in the viscous flow

System no.	Bubble phase 1	Continuous phase 2	η_2 (P)	p	γ (dyn cm^{-1})	$\Delta\rho$ (g cm^{-3})
1	Air	Silicone oils 1000 to 30,000*	1·10 to 333	0	20·3†	−0·970†
2	Air	Ucon oils‡ {LB 285 / LB 1715}	{1·30 / 8·41}	0	30·8†	−0·990†
3	Air	{60 % dibutyl phthalate / 40 % Ucon oil LB 1715‡}	1·40	0	—	−1·026
4	Air	84 % glycerol	0·92	0	65·3	−1·219
5	Air	84 % glycerol + 0·03 % Aerosol O.T.§	0·96	0	45·6	−1·220
6	Air	84 % glycerol + 0·12 % Aerosol O.T.§	0·96	0	33·4	−1·220
7	Air	Silicone oils 2 to 20*	0·025 to 0·22	0	19·4†	−0·922†
8	Air	Water	0·01	0	71·6	−0·998
9	Air	Water + 0·2 % Tween 20‖	0·01	0	32·3	−0·998
10	Water + 16 to 42 % $Cd(NO_3)_2$	Ucon oils‡ {LB 285 / LB 1715}	{1·30 / 8·41}	{$1·2\times10^{-3}$ / $7·5\times10^{-3}$}	5·6 to 8·6	0·169 to 0·485
11	Ucon oil LB 285‡	86 % glycerol	1·224	1·1	—	−0·214
12	Silicone oils* {1000 / 5000}	86 % glycerol + 0·5 % Tween 20‖	1·224	{8·3 / 41·6}	—	−0·254

* Dow Corning fluid, 200 series.
† Average values.
‡ Union Carbide polyglycol oil.
§ Sodium dioctyl sulfosuccinate (American Cyanamid Co.).
‖ Polyoxyethylene sorbitan monolaureate, oil in water emulsifier.

TABLE 1. Properties of fluid systems (22 ± 0·5 °C).

region ($Re < 1$) of which systems 11 and 12 were used for the experiments at high p. Systems 7 to 9 yielded high $Re(> 20)$. The interfacial tensions were lowered by the addition of surfactants to the continuous phase (systems 5 and 6). In systems 12 surfactant was added to avoid wetting of the glass by the bubbles.

All experiments were conducted in a room maintained at $22{\cdot}0 \pm 0{\cdot}5$ °C. Strict precautions were taken with the cleaning of all glassware to avoid wetting or sticking of the bubbles to the glass wall of the tubes. The viscosities of the liquids used were measured in thermostated ($22{\cdot}00 \pm 0{\cdot}01$ °C) capillary ($\eta < 10$ P) and rotational ($\eta > 50$ P) viscometers. The surface and interfacial tensions of the systems were determined by the ring-pull and pendant-drop methods, respectively.

4. Results and discussion

4.1. *Viscous flow*

(*a*) *General observations.* In all systems studied (no. 1 to 6 and 10 to 12) the film thickness remained constant between the leading and rear ends of the air and liquid bubbles. This includes those systems (no. 5, 6 and 12) in which surfactant was present in the continuous phase. The Reynolds number $Re = (RV_b\rho_2)/\eta_2$ in these experiments varied from 10^{-5} to 1·0, and the dimensionless group $(\eta_2 V_b/\gamma)$ from 2×10^{-4} to 2×10^{-2}. Visual observation inside the film with tracer particles added to the continuous phase indicated velocity profiles qualitatively in accord with those given in figures 1(*a*) and (*b*) for bubbles in systems of $p > 0$ and $p = 0$, respectively. The profiles were studied quantitatively and the results are reported below. When the liquid bubbles of systems 10 to 12 contained tracer particles, internal circulation patterns were observed having the general pattern predicted; these are illustrated schematically in figure 2(*a*) and are analogous to those reported (Linton & Sutherland 1957; Garner & Haycock 1959) for falling spherical liquid drops in viscous fluids. The droplets moved fastest (relative to the bubble) when the path was parallel to the tube axis and slowest when it changed direction at the bubble ends.

(*b*) *Viscosity ratio* $p = 0$.

(i) *Bubble length.* In a given system h and V_b were independent of l_b, provided that $l_b > 2R$, including the infinite air bubble.

(ii) *Film thickness.* The results obtained with the air and liquid bubble systems for three values of R are shown in tables 2 and 3, respectively. It can be seen that the observed values of h, corrected for refraction error, are in good agreement with those calculated from (19), using the experimentally determined η_2, V_b and $\Delta\rho$. In most cases h was between 10 and 25 % of the tube radius so that (22) did not apply. That the agreement reached after applying the refraction correction was not fortuitous was shown by system 3 where phase 2 had the same refractive index as glass. Equation (19) also applied to the infinite air bubble.

(iii) *Viscosity and interfacial tension.* As table 2 shows for rising air bubbles, when γ and R were constant, h remained unchanged over a wide range of viscosities. The quantity $(V_b\eta_2/\Delta\rho)$ shown in the last column at each R was constant for a given R and γ (Barr 1926), and independent of η_2. A closer examination of the

System	γ (dyn cm^{-1})	η_2 (P)	ρ_2 (g cm^{-3})	R = 0·400 cm: h_{expt}* (μ)	h_{calc}† (μ)	$V_b\eta_2/\Delta\rho$ (cm^3 sec^{-2})	R = 0·300 cm: h_{expt}* (μ)	h_{calc}† (μ)	$V_b\eta_2/\Delta\rho$ (cm^3 sec^{-2})	R = 0·200 cm: h_{expt}* (μ)	h_{calc}† (μ)	$V_b\eta_2/\Delta\rho$ (cm^3 sec^{-2})
1	20·2	1·10	0·967	1145	1160	3·66	750	765	1·34	270	305	0·11
	20·4	10·54	0·972	1165	1195	4·06	750	780	1·43	280	300	0·10
	20·5	52·8	0·972	1185	1190	3·99	775	775	1·40	295	290	0·09
	20·5	333	0·974	1175	1190	4·03	760	775	1·41	—	—	—
2	30·6	1·30	0·986	1070	1070	2·84	630	640	0·74	130	100	0·01
	31·1	8·41	0·998	1080	1095	3·04	625	635	0·71	130	100	0·01
3‡	—	1·40	1·026	1070	1070	2·82	635	640	0·74	—	—	—
6	33·4	0·96	1·220	855	855	1·36	515	520	0·38	(95)§	(150)§	(0·01)§
5	46·6	0·96	1·220	860	865	1·43	415	380	0·16	No bubble flow		
4	65·3	0·91	1·219	845	855	1·36	370	365	0·14	No bubble flow		
Mean h_{expt}/h_{calc}				0·991			0·992			1·009		

* Measured value corrected for refraction error.
† Equation (19).
‡ Liquid of same refractive index as glass.
§ Bubble tended to stick to tube wall.

TABLE 2. Film thicknesses for air bubbles: viscous flow.

data reveals that there is a very small increase in h and $(V_b \eta_2/\Delta\rho)$ as $\Delta\rho$ increases in both systems 1 and 2. As the surface tension increases down table 2, h at each tube radius decreases. Exceptions to this trend are systems 4 and 5 at $R = 0{\cdot}4$ cm. These results were used to construct a dimensionless plot according to (23) which

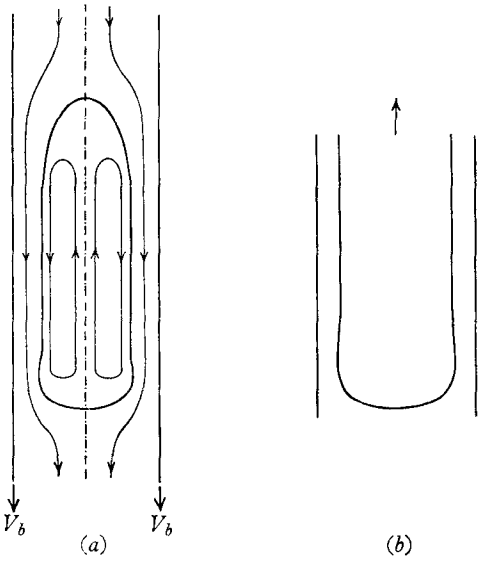

FIGURE 2. (*a*) Schematic drawing of streamlines in rising bubble and surrounding film; $p > 0$. To simplify the representation, the bubble is brought to rest by moving the tube with velocity V_b. (*b*) Tracing of photograph of wave disturbance at trailing end of rising liquid bubble; system 12, $p = 8{\cdot}3$.

γ (dyn cm^{-1})	η_2 (P)	$\Delta\rho$ (g cm^{-3})	h_{expt}* (μ)	h_{calc}† (μ)	$V_b \eta_2/\Delta\rho$ (cm^3 sec^{-2})
5·6	1·30	0·348	1245	1215	4·31
6·2	1·30	0·485	1280	1255	4·81
7·4	8·41	0·169	1010	1000	2·24
8·2	8·41	0·337	1185	1175	3·82
8·6	8·41	0·471	1240	1220	4·36
		Mean h_{expt}/h_{calc}		1·016	

* Measured value corrected for refraction error.
† Equation (19).

TABLE 3. Film thickness for falling liquid bubbles: viscous flow. System 10, $R = 0{\cdot}400$ cm.

is shown in figure 3. The experimental points lie on a single curve with a positive intercept $(K/\gamma) = 5{\cdot}0$. This implies that for a given system there exists a tube diameter below which the bubble will stick; this was observed in systems 4 and 5 at $R = 0{\cdot}2$ cm. Included in figure 3 is a curve which was constructed by Barr (1926) from his own data and those of Abrams, Kavanagh & Osmond (1921) and Faust (1919). It will be noted that at a given (K/γ) the values of $(V_b \eta_2/K)$ obtained by these authors are somewhat higher than the present ones. Barr

found that flow ceases at a value of (K/γ) of approximately 0·6, whereas Bretherton (1961) has shown from experiment that bubble flow becomes unsteady or stops at $(K/\gamma) < 3{\cdot}37$.

For the liquid bubbles (system 10, table 3) increasing $\Delta\rho$ by adding cadmium nitrate to the water caused a marked increase in h. While γ was nearly constant $(V_b \eta_2/\Delta\rho)$ showed substantial variation.

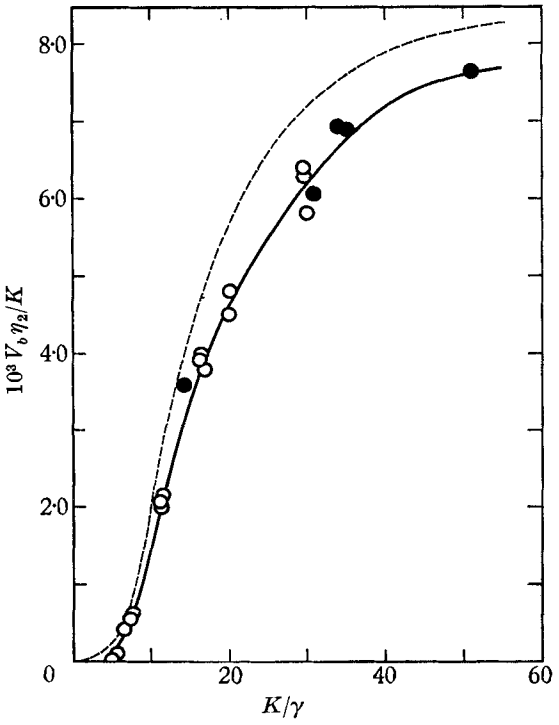

FIGURE 3. Plot according to the dimensionless equation (23). Experimental points are open circles (rising air bubbles) and closed circles (falling inviscid liquid bubbles). The broken line is that constructed by Barr (1926) from his own and other data.

Equation (23) also applied to the liquid bubbles (figure 3). It was noted that when aqueous cadmium nitrate bubbles were introduced into silicone oils the bubbles ceased to flow after a short time because they had wetted the glass wall. This behaviour can be explained by the high γ (45 dyn cm^{-1}) which yielded $K/\gamma = 6{\cdot}5$, close to the intercept where flow is predicted to cease.

(iv) *Velocity profile in film.* The measured velocity profile was compared with that given by (18) for both finite and infinite air bubbles rising in silicone oil. The results are shown graphically in figure 4. There was no significant difference in the profile for the finite and infinite bubbles and the agreement with theory was excellent.

(v) *Bubble shape.* The ends of the bubbles were spheroidal with the leading end prolate ($r_e > 1$) and the trailing end generally oblate ($r_e < 1$) and the axis of revolution coincident with the tube axis. An exception was system 4, in which both ends were prolate. Figure 5(*a*) shows an air bubble rising in Ucon oil

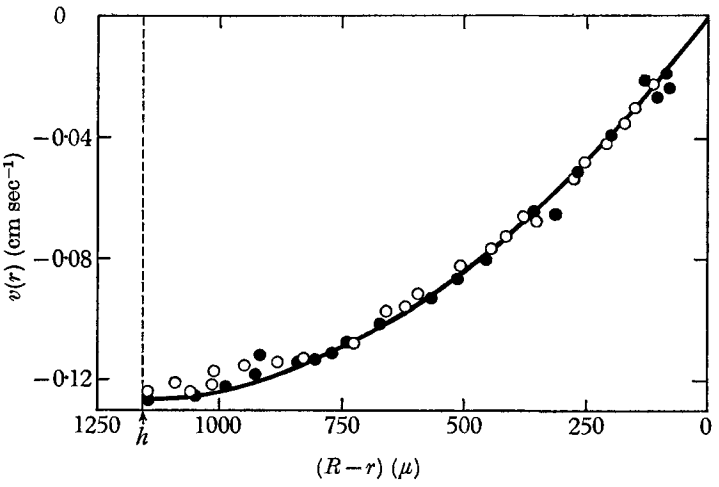

FIGURE 4. Velocity profile in film surrounding rising air bubbles, system 2. Experimental points are open circles (air bubbles 3·0 to 6·0 cm long) and closed circles (infinite air bubbles). The line drawn is calculated from (18). The velocity gradient G at the interface is zero.

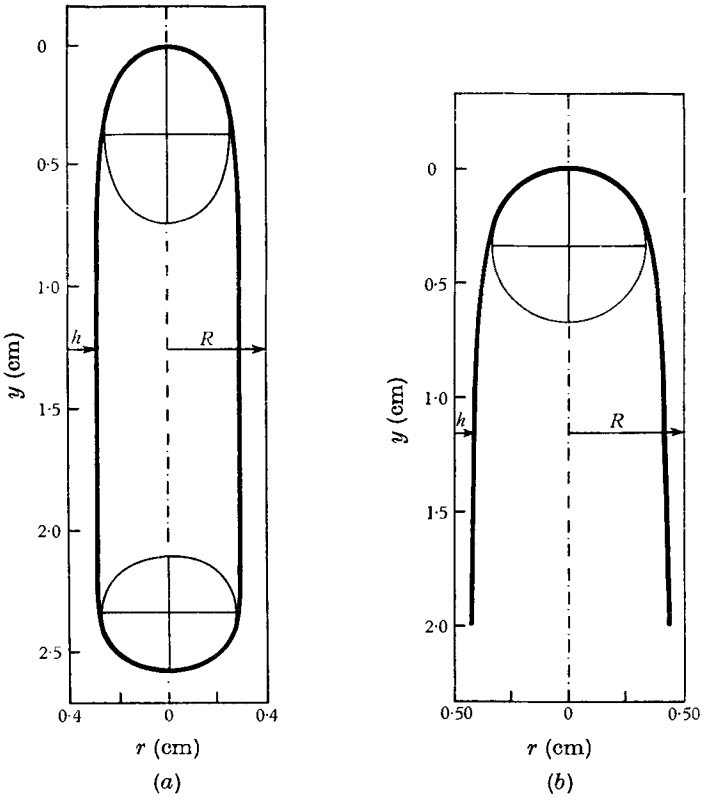

FIGURE 5. Contours of bubble ends traced from photographs. (*a*) Rising air bubble; system 2; $\eta_2 = 8{\cdot}41$ P. Viscous flow. (*b*) Advancing end of infinite air bubble rising in Silicone oil; $\eta_2 = 0{\cdot}05$ P. Inertial flow.

(system 2) as traced from photographs together with the best-fit ellipse, from which the axis ratio r_e = (axis of revolution/diametrical axis) was calculated for each end. The values of r_e calculated this way for several systems are recorded in table 4. The contours were unaffected by bubble length; the r_e of the leading end increased and that of the trailing end decreased with increasing γ. The axis ratios at fixed γ were independent of η_2.

System	γ (dyn cm^{-1})	η_2 (P)	Axis ratio r_e	
			Leading end	Rear end
1	20·2	1·10	1·36	0·77
	20·4	10·54	1·28	0·78
	20·5	52·8	1·28	0·78
2	30·6	1·30	1·41	0·71
	31·1	8·41	1·39	0·72
4	65·3	0·92	1·68	1·36

TABLE 4. Shapes of air bubbles: viscous flow, R = 0·400 cm.

System	p	V_b (cm sec^{-1})	$h(\mu)$		$h_0(\mu)$	
			expt.*	cal.†	expt.*	calc.†
11	1·02	0·183	1015	1010	650 ± 50	660
12	8·3	0·092	1010	1015	510 ± 50	505
	41·6	0·109	1170	1170	580 ± 50	540

* Measured value corrected for refraction error.
† From equation (11) using the measured V_b, η and ρ.
‡ From equation (16) using the measured V_b, η and ρ.

TABLE 5. Rising liquid bubbles: viscous flow, $p > 0$, R = 0·400 cm.

The air bubbles showed a small wave disturbance at the initial point of curvature of the rear end. The amplitude of the wave was observed to be of the order of 20 μ in system 2 (h = 1080 μ) and thus too small to be shown in figure 5(*a*). Much greater amplitudes were observed in liquid bubbles (systems 10 to 12) as shown by the tracing of a photograph (figure 2(*b*)) of the rear end of a silicone oil bubble.

(*c*) *Viscosity ratio* $p > 0$. Film thickness and velocity profile measurements were made in systems 11 and 12, and it was these results which provided the most convincing proof of the theory presented in § 2.1.

Table 5 shows the agreement between calculated and measured values of h and h_0.

The profiles in the bubble and the film were made in system 11, and in the film alone in system 12. The experimental points, shown in figure 6 fall very close to the theoretical lines.

4.2. *Inertial flow*

The rates of rise of the upper end of the infinite air bubble in a freely emptying tube (R = 0·5 cm) were measured for a number of low viscosity silicone oils and water (systems 7 to 9). The values of β given by (26) were calculated and are

shown in table 6 together with the Reynolds number. For the silicone oils having a low surface tension the values of β fell off only slightly from the maximum 0·47 (theoretical value = 0·46 to 0·49) as the viscosity was increased from 2 to 20 cP. With water, although Re was much greater than in the silicone oil system, β was appreciably smaller. Upon the addition of a surfactant β increased but did not reach the theoretical value. Davies & Taylor (1950), also using water, found that

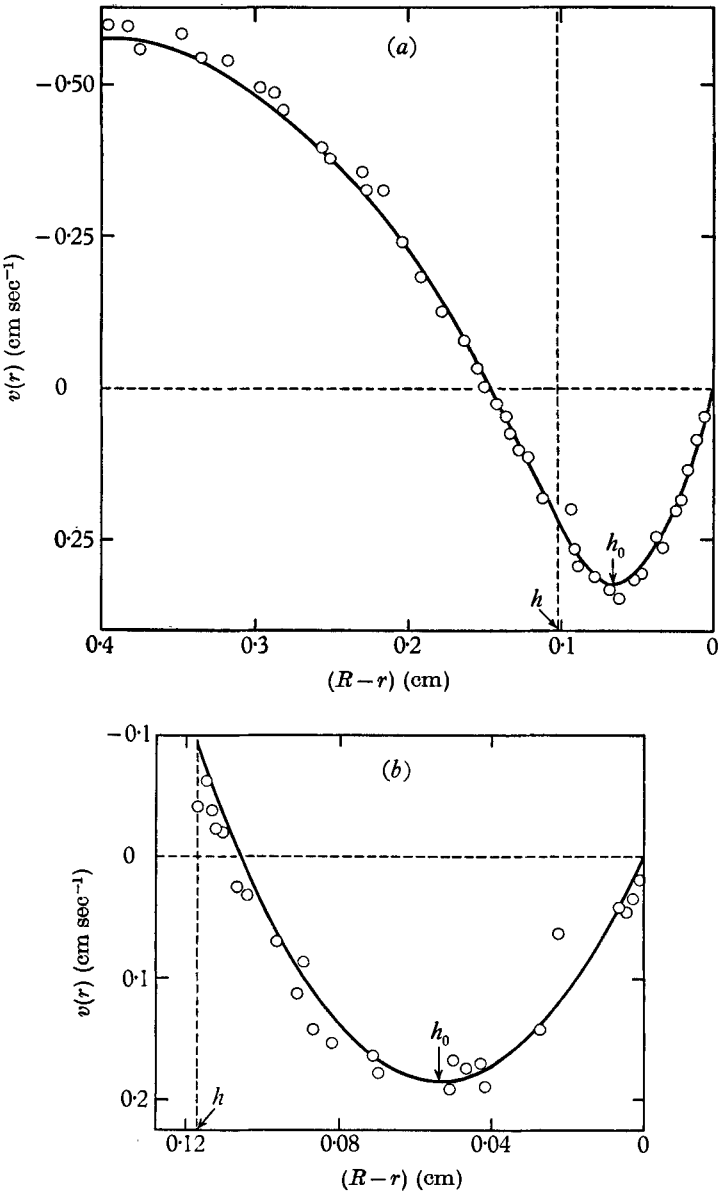

FIGURE 6. Rising liquid bubbles. (*a*) Velocity profile in bubble and surrounding film; system 11; p = 1·1. (*b*) Velocity profile in film; system 12; p = 41·6. The curves drawn are calculated from (9) and (10) using values of A_2 and H calculated from (12) and (13), respectively.

the theoretical value of β was not reached until $Re = 1600$, an effect which may be attributed to the high surface tension of the water.

The leading ends in these systems were found to be spherical (figure 5(*b*)) as assumed in the theory (Davies & Taylor 1950). From the photographs, the film thickness (corrected for refraction error) was obtained for a distance of 2 cm

System	γ (dyn cm^{-1})	η_2 (P)	$Re = RV_b\rho_2/\eta_2$	β equation (26)
7	18·7	0·025	240	0·47
	19·5	0·056	100	0·47
	20·1	0·12	45	0·46
	21·9	0·22	20	0·42
8	71·6	0·01	375	0·33
9	32·3	0·01	440	0·38

TABLE 6. Air bubbles at high Reynolds numbers, $R = 0{\cdot}500$ cm.

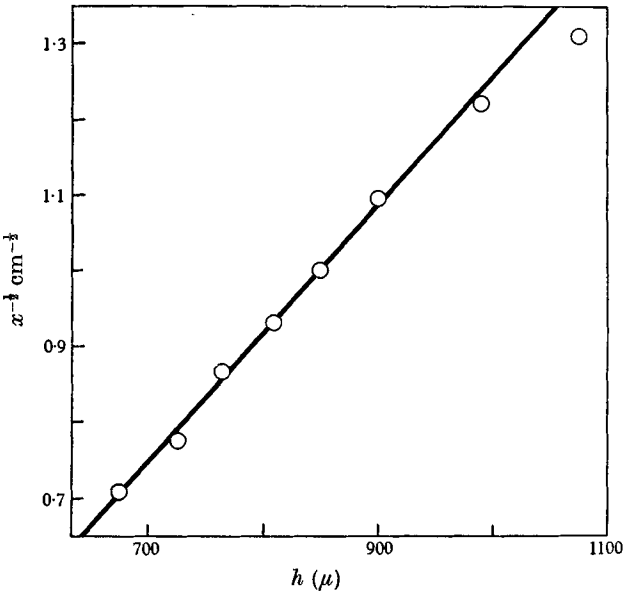

FIGURE 7. Variation of film thickness with distance for a rising air bubble in silicone oil $\eta_2 = 0{\cdot}05$ P. The line drawn is the best-fit of the experimental points.

below the vertex; figure 7 shows a plot of h vs $x^{-\frac{1}{2}}$. The mean value of β calculated from plots of this kind by means of (27) was 0·93; as also found by Davies & Taylor (1950) these values are higher than those calculated from V_b (table 6). This discrepancy probably arises from the neglect of the boundary layer at the wall of the tube leading to an overestimate in v_2 and hence β in (27).

Some experiments were also carried out at lower Re (20 to 75) using systems 8 and 9 with $R = 0{\cdot}3$ cm. Here, the bubbles consisted of a leading portion of greater diameter in which h was constant, and a tail of smaller diameter and variable h, the tail exhibiting wave disturbances which appeared as successive thick rings. Barr (1926) has described this phenomenon in some detail. It was found that the

values of h_{expt} for the front portion of the bubble were about half those calculated from the measured V_b using (19), and that the values of β (0·04 to 0·15) were very much lower than the theoretical value, indicating that both viscous and inertial effects contributed to the flow.

5. Concluding remarks

The results obtained in the viscous flow region have shown good agreement with (9), (10) and (11) and those in the inertial flow region with (26).

The discovery that at a given K and γ the shape of the bubble ends and h, and hence the total deformation of the bubble, were independent of η_2 was surprising. In spite of this simplification, however, it is thus far impossible to calculate V_b *a priori* in viscous systems. As would be expected, the deformation changed with increasing γ and decreasing h whilst the shapes of the bubble ends (system 4 excepted) became more eccentric. Equation (23) accounts qualitatively for the results obtained, i.e. at a given K and γ, $(V_b \eta_2)$ was constant and as γ increased V_b decreased.

With viscous bubbles ($p > 0$) internal circulation was observed and the measured velocity profiles indicated unhindered transmission of shear stress across the interface, despite the presence of surfactant in the continuous phase which might be expected to impede internal circulation (Rumscheidt & Mason 1961). However, the continual renewal of the interface as the bubble moves through the viscous liquid may prevent the build-up of the elastic interfacial film necessary to inhibit internal circulation by balancing some of the shear stress at the interface and thus upsetting (7). The absence of this film may also be responsible for the result noted in systems 4 to 6 ($p = 0$) where h remained unaffected by the increase in γ at high V_b (1·4 cm sec^{-1}), whereas at low V_b (0·15 to 0·4 cm sec^{-1}) h decreased with increasing γ.

When internal circulation is impeded in viscous bubbles, the boundary conditions are as before except for (7) which is replaced by

$$-\eta_1\left(\frac{\partial v_1}{\partial r}\right)+\frac{d\gamma}{dx}=-\eta_2\left(\frac{\partial v_2}{\partial r}\right), \tag{28}$$

where the gradient in interfacial tension expresses the elastic response of the interface (Rumscheidt & Mason 1961). Again assuming parallel flow, an assumption which may not be valid if $(d\gamma/dx)$ is large, equations similar to (9), (10) and (11) may be derived which make it possible to calculate $(d\gamma/dx)$ from measured velocity profiles. These equations, which are not reproduced here, suggest a possible technique for studying dynamic interfacial film properties in systems which may be found to exhibit impeded transmission of the fluid shear stress across the interface. Such impedance was observed in flowing bubbles in systems containing surfactants (Goldsmith & Mason 1962*b*).

This work was supported (in part) by research grant H–5911 from the National Heart Institute of the United States Public Health Service. One of us (H. L. G.) was the holder of a Union Carbide Fellowship (1959–60) and the Spruce Falls Power and Paper Company Limited Fellowship (1960–61).

REFERENCES

ABRAMS, V. R., KAVANAGH, J. T. & OSMOND, C. H. 1921 *Chem. Met. Eng.* **25**, 665.
BARR, G. 1926 *Phil. Mag.* **1**, 395.
BRETHERTON, F. P. 1961 *J. Fluid Mech.* **10**, 166.
DAVIES, R. M. & TAYLOR, G. I. 1950 *Proc. Roy. Soc.* A, **200**, 375.
DUMITRESCU, D. T. 1943 *Z. angew. Math. Mech.* **23**, 139.
DUKLER, A. E. & BERGELIN, O. P. 1952 *Chem. Engng Progr.* **48**, 557.
FAUST, O. 1919 *Z. Phys. Chem.* **93**, 758.
GARDESEN, I. I. 1930 *Oil Gas J.* **28**, 115.
GARNER, F. H. & HAYCOCK, P. J. 1959 *Proc. Roy. Soc.* A, **252**, 457.
GAVELIN, G. 1954 *Pulp Pap.* (*Mag.*) *Can.* **55** (3), 191.
GIBSON, A. H. 1913 *Phil. Mag.* **26**, 952.
GOLDSMITH, H. L. & MASON, S. G. 1962*a* *J. Colloid Sci.* **17**, 443.
GOLDSMITH, H. L. & MASON, S. G. 1962*b* *J. Colloid Sci.* (in the Press).
GRIMLEY, S. S. 1945 *Trans. Instn Chem. Engrs, Lond.*, **23**, 228.
LINTON, M. & SUTHERLAND, K. L. 1957 *Second International Congress on Surface Activity*, Vol. 1, p. 494 *et seq.* London: Butterworth.
MARCHESSAULT, R. H. & MASON, S. G. 1960 *Industr. Engng Chem.* **52**, 79.
MARSHALL 1917 *Explosives*, Vol. II. London: Churchill.
NUSSELT, O. 1916 *Z. Ver. dtsch. Ing.* **60**, 541.
RICHARDSON, E. G. 1953 *J. Colloid Sci.* **8**, 367.
RUMSCHEIDT, F. D. & MASON, S. G. 1961 *J. Colloid Sci.* **16**, 210.
SCHULZ, H. S. 1929 *Chem. Fabr.* 497.